2 cm spatial-resolution and 2 km range Brillouin optical fiber sensor using a transient differential pulse pair

Yongkang Dong,[1,2] Hongying Zhang,[1] Liang Chen,[1] and Xiaoyi Bao[1,*]

[1]Fiber Optics Group, Department of Physics, University of Ottawa, Ottawa, K1N 6N5, Canada

[2]e-mail: aldendong@gmail.com

*Corresponding author: Xiaoyi.Bao@uottawa.ca

We report a high-spatial-resolution and long-range distributed temperature sensor through optimizing differential pulse-width pair Brillouin optical time-domain analysis (DPP-BOTDA). In DPP-BOTDA, the differential signal suffers from a signal-to-noise ratio (SNR) reduction with respect to the original signals, and for a fixed pulse-width difference the SNR reduction increases with the pulse width. Through reducing the pulse width to a transient regime (near to or less than the phonon lifetime) to decrease the SNR reduction after the differential process, the optimized 8/8.2 ns pulse pair is applied to realize a 2 cm spatial resolution, where a pulse generator with a 150 ps fall-time is used to ensure the effective resolution of DPP-BOTDA. In the experiment, a 2 cm spatial-resolution hot-spot detection with a 2 °C temperature accuracy is demonstrated over a 2 km sensing fiber.   © 2012 Optical Society of America

OCIS codes: 280.4788, 290.5900.

1. Introduction

For two decades, distributed Brillouin optical fiber sensors have gained much interest for their potential capabilities of monitoring temperature and strain, which find applications in civil and structural engineering, environmental monitoring, geotechnical engineering, and similar fields. Brillouin optical time-domain reflectometry (BOTDR) [1–3] and Brillouin optical time-domain analysis (BOTDA) [4,5] have been proposed for effective distributed sensing. BOTDR makes use of spontaneous Brillouin scattering with the advantage of only one-end access, while BOTDA is generally built up in a loop configuration for counterpropagating pump and probe waves to create stimulated Brillouin scattering (SBS) featuring a much better signal-to-noise ratio (SNR). However, for both cases, there is a trade-off between the spatial resolution and the measurement accuracy. The spatial resolution is determined by the pulse width and can be improved by using a short pulse;

meanwhile a short pulse will give a broadened Brillouin gain spectrum (BGS) and a weak Brillouin signal, especially when it is smaller than the phonon lifetime (∼10 ns in silica fiber). These restrictions prohibit one from improving the spatial resolution through simply shortening the pulse width [6]. Generally, it is accepted that the spatial resolution is no better than 1 m for conventional Brillouin time-domain sensors.

In recent years, much attention has been paid to improving the spatial resolution, and several novel techniques have been proposed. Such progresses bring the spatial resolution to the order of cm and even mm [7–17]. Among these techniques, there is one kind sharing the common working principle of preexcitation of a weak acoustic wave [7–11], which was first observed in [7]. In this technique, a preexcitation acoustic field is created via electrostriction through the interference of a weak CW pump wave and a counterpropagation CW signal wave, and then a very short pulse or dark pulse can be applied to obtain a high spatial resolution. However, with this kind of technique, it is expected that the sensing range is limited by the pump depletion. Using a

finite-duration prepump [10] or a dark base [11] can overcome the pump depletion and thus extend the sensing range; however, due to the contribution from the prepump wave on the spectrum, there could be a frequency error in the case of a small strain or temperature change over a short section length.

More recently, a novel differential technique has been proposed, in which two separate measurements are implemented with two different pulses, and the differential signal is obtained by making subtraction between the two Brillouin signals [13,14]. A high spatial resolution can be achieved by using a small pulse-width difference of the pulse pair. The differential technique can be realized by two methods: π-phase-shift pulse pair [13] and differential pulse-width pair (DPP) [14]. In the π-phase-shift pulse pair, two pulses share the same pulse width, except that the last portion of the second pulse is phase inverted (with π phase shift); the DPP simply uses two pulses with different pulse widths. Both techniques have shown the capabilities of high spatial resolution and long-range sensing [18,19].

In this paper, we first theoretically investigate the DPP-BOTDA signal, and the simulation results show that the differential signal suffers from a reduction in SNR with respect to the two original signals, which indicates that the spatial resolution cannot be improved through always reducing the pulse-width difference of the pulse pair in terms of the SNR. In the experiment, we present an optimized scheme by reducing the DPP to a transient domain to obtain a cm-order spatial resolution. Using the 8/8.2 ns pulse pair, we achieve a 2 cm spatial resolution with a 2 °C temperature accuracy over a 2 km length, which, to the best of our knowledge, is the best performance in such a length for BOTDA systems.

2. Theoretical Description and Simulations

The SBS process can be described by one-dimensional coupled wave equations involving a backward pump wave ($-z$ direction), a forward Stokes wave ($+z$ direction), and a backward acoustic wave. Under the slowly varying envelope approximation, the three-wave coupled wave equations are written as [20]

$$-\frac{\partial E_p}{\partial z} + \frac{n}{c}\frac{\partial E_p}{\partial t} = ig_2 E_s Q, \qquad (1a)$$

$$\frac{\partial E_s}{\partial z} + \frac{n}{c}\frac{\partial E_s}{\partial t} = ig_2 E_p Q^*, \qquad (1b)$$

$$\frac{\partial Q}{\partial t} + \Gamma Q = i\frac{g_1}{\eta}E_p E_s^*. \qquad (1c)$$

Here E_p, E_s, and Q are field amplitudes of the pump wave, Stokes wave, and acoustic waves, respectively; n is the refractive index of the optical fiber; c is the light speed in vacuum; $\Gamma = \Gamma_B/2 + i\Delta\Omega$; $\Gamma_B/2\pi$ is the

Brillouin gain linewidth (FWHM); $\Delta\Omega = (\omega_p - \omega_S) - \Omega_B$ is the detuning from the Brillouin frequency shift (BFS); and ω_p, ω_S, and Ω_B are the annular frequencies of the pump, Stokes, and Brillouin shift, respectively. In Eqs. (1), E_p and E_s are normalized so that $|E_p|^2$ and $|E_S|^2$ are the optical intensity of the pump and Stokes waves, respectively.

Integrating Eq. (1c) gives

$$Q = i\frac{g_1}{\eta}\int_0^t E_p E_s^* \exp[-\Gamma(t-\tau)]\mathrm{d}\tau. \qquad (2)$$

Substituting Eq. (2) into Eqs. (1a) and (1b), we have

$$-\frac{\partial E_p}{\partial z} + \frac{n}{c}\frac{\partial E_p}{\partial t} = -\frac{g_0\Gamma}{2}\int_0^t E_p E_s^* \exp[-\Gamma(t-\tau)]\mathrm{d}\tau,$$

$$\frac{\partial E_s}{\partial z} + \frac{n}{c}\frac{\partial E_s}{\partial t} = \frac{g_0\Gamma}{2}\int_0^t E_p^* E_s \exp[-\Gamma^*(t-\tau)]\mathrm{d}\tau, \qquad (3)$$

where $g_0 = 4g_1 g_2/(\eta\Gamma_B)$ is the Brillouin gain coefficient. Equation (3) can be used to numerically solve the evolution of the pump and Stokes waves in an optical fiber. We use the following parameters to do the numerical simulation in a standard single-mode fiber: $L = 10$ m, $\lambda = 1550$ nm, $A_{eff} = 50$ μm^2, $\Gamma_B/2\pi = 30$ MHz, and $g_0 = 2.5 \times 10^{-11}$ m/W.

The DPP-BOTDA is implemented as follows: first, two time traces of the Brillouin signal are obtained by using two pulses with different pulse widths; second, the differential signal is obtained by taking subtraction between the two Brillouin signals; then the differential Brillouin spectra can be obtained by sweeping the frequency offset in the vicinity of the BFS. The DPP-BOTDA features a high spatial resolution, which is determined by the pulse-width difference of the differential pulse pair. With the frequency offset tuned to the BFS of the optical fiber, Fig. 1 shows the time traces of the Brillouin signal at the start region of the fiber with a 8/8.2 ns pulse pair, which is used in the following experiment. The 8 and 8.2 ns pulses give 80 and 82 cm spatial resolutions in an optical fiber, respectively, which can be seen from the rising edges of the Brillouin signal at the transition region. Note that the two signals with 8 and 8.2 ns pulses totally overlap at the beginning 8 ns section, and the spatial-resolution improvement is clearly shown on the curve of differential signal, in which a 0.2 ns rising edge of the signal indicates a 2 cm spatial resolution.

As seen in Fig. 1, the improving spatial resolution of the differential signal is at the expense of a reduction of signal or SNR, which is the limitation of further improving the spatial resolution through shortening the pulse-width difference of the differential pulse pair. We define the SNR reduction of DPP-BOTDA as

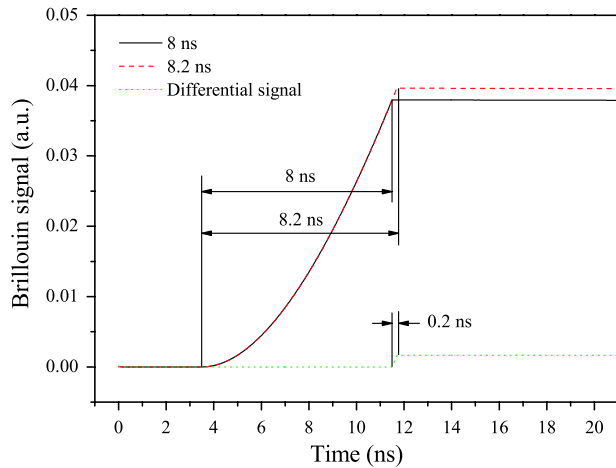$$R_{SNR} = -10\log\frac{I_{\tau 2} - I_{\tau 1}}{I_{\tau 1}}, \qquad (4)$$

Fig. 1. (Color online) Time traces of the Brillouin signal in the vicinity of start region of the fiber with 8 and 8.2 ns pulse widths and their differential signal.

where $I_{\tau 1}$ and $I_{\tau 2}$ are the Brillouin signal intensities with the pulse widths of τ_1 and τ_2, respectively, where τ_2 is longer than τ_1. Figure 2 shows the SRN reduction of DPP-BOTDA as a function of the pulse-width τ_1 for the pulse-width differences of 0.1 and 0.2 ns, respectively. It is seen that smaller pulse-width difference experiences larger SRN reduction, and the SRN reduction for the 0.1 ns pulse-width difference is about 3 dB larger than that for the 0.2 ns for the pulse-width τ_1 ranging from 2 to 20 ns. Generally, in DPP-BOTDA, a long pulse pair with a small pulse-width difference is used to achieve an improved spatial resolution with a narrow Brillouin spectrum. On one hand, note that for a fixed pulse-width difference, the SRN reduction increases with the pulse width, so a short pulse pair is preferable to decrease the SRN reduction; on the other hand, a short pulse will broaden the Brillouin spectrum, leading to a large frequency uncertainty. So for a high spatial resolution with a fixed, small pulse-width difference for
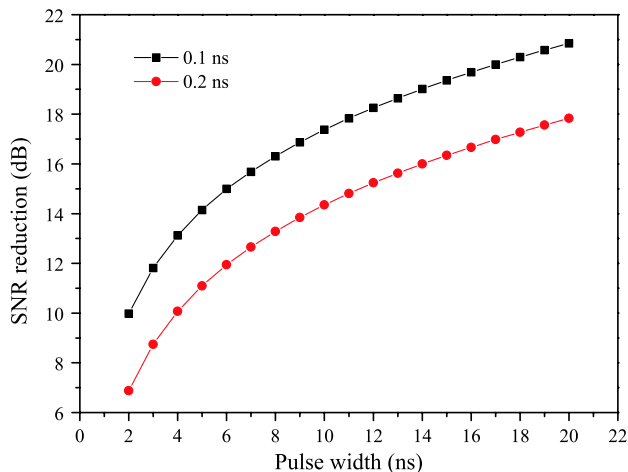

Fig. 2. (Color online) SRN reduction of DPP-BOTDA as a function of the pulse width (the short pulse of the pulse pair) for the pulse-width differences of 0.1 and 0.2 ns, respectively.

a real system, an optimal pulse pair should be carefully chosen by considering the trade-off between the SRN reduction and Brillouin spectrum broadening.

3. Experimental Setup

The experimental setup is shown in Fig. 3. Two narrow-linewidth fiber lasers operating at 1550 nm are used to provide the pump and probe waves, whose frequency difference is locked by a microwave frequency counter. A pulse generator is used to generate the pump pulse, which is amplified by an erbium-doped fiber amplifier (EDFA) before being launched into the sensing fiber. A piece of 10 m polarization-maintaining (PM) fiber is used as sensing fiber to avoid polarization-dependent fluctuation, and its BFS is 10 820 MHz at 25 °C. A 3.5 GHz bandwidth detector with a transition time (10%–90%) of 115 ps is used to detect the Brillouin signal, which can resolve the cm variation in strain or temperature. The sampling rate of the digitizer is set at 10 GHz/s, which corresponds to 1 cm/point. A semiconductor Peltier heater is applied to create a hot spot on the sensing fiber, as shown in Fig. 3.

4. Experimental Results and Discussion

A. Limitation of Actual Spatial Resolution of DPP-BOTDA

A subnanosecond pulse-width difference can be applied to obtain a cm-order spatial resolution, while the pulse widths of the pulse pair should be carefully chosen by considering the trade-off between the SRN reduction of DPP-BOTDA and Brillouin spectrum broadening for a real system as discussed in the second section. In our system, an optimized 8/8.2 ns pulse pair, which provides the best performance for the fixed 0.2 ns pulse-width difference, is used to achieve a 2 cm spatial resolution.

Nominally, the spatial resolution of DPP-BOTDA is determined by the pulse-width difference of the pulse pair when ideal rectangular pulses are applied. However, the actual spatial resolution would be limited by the fall-time of the pulses, which limits the available minimum duration of the differential pulse. We first investigate the limitation of actual spatial resolution of DPP-BOTDA by using two pulse generators with different bandwidths. The pulse waveforms of 8 and 8.2 ns pulses generated from pulse generator 1 are plotted in Fig. 4(a), and they exhibit a 780 ps fall-time (10%–90%). The differential pulse, which is plotted as the green curve and is obtained by subtracting between the two pulse waveforms, shows a 500 ps pulse width (FWHM). The pulses generated from pulse generator 2, as shown in Fig. 4(b), have a 150 ps fall-time (10%–90%), and the differential pulse of 8 and 8.2 ns pulses shows a 200 ps pulse width (FWHM), which is the same as the pulse-width difference of the pulse pair.

The frequency offset between the pump and probe waves was swept from 10 660 MHz to 10 990 MHz with a step of 10 MHz. Using a 0.5 mW probe and a 500 mW pump pulse, each time trace of the
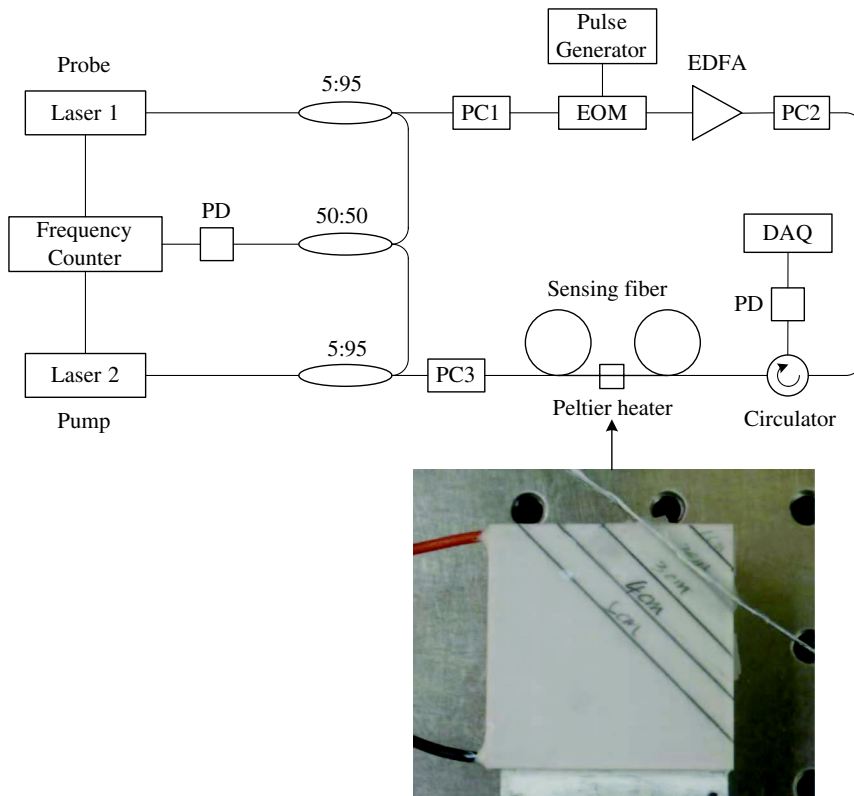
Fig. 3. (Color online) Experimental setup. PD, photodetector; PC, polarization controller; EOM, electro-optic modulator; EDFA, erbium-doped fiber amplifier; DAQ, data acquisition. The surface of the Peltier heater is marked with lines from 1 to 5 cm.

Brillouin signal was recorded by averaging a number of 1000 to reduce the noise. With a 5 cm segment located at 4.31 to 4.36 cm heated to 73 °C, two separate measurements were carried out with the two pulse generators. The measured three-dimensional (3-D) Brillouin spectra of DPP-BOTDA with the 8/8.2 ns pulse pair are shown in Fig. 5. We see that both spectra clearly manifest the heated segments with a high SNR. The fitted BFS and the corresponding temperature of the two cases are plotted in Fig. 6, where the blue solid line represents the real temperature profile. Comparing the results with the two pulse generators, it is clear that the temperature profile

obtained with pulse generator 2 is closer to the real temperature profile; the temperature profile obtained with pulse generator 1 is broadened, and its rising edge (10%–90%) indicates an effective spatial resolution of 5 cm, which is determined by the 500 ps pulse width of the differential pulse rather than the 200 ps pulse-width difference of the 8/8.2 ns pulse pair.

B. 2 cm Hot-spot Detection over 2 km Range

We then carried out measurements with the 8/8.2 pulse pair using pulse generator 2 for 2 cm hot-spot detection. A 2 cm segment located at 4.33 to 4.35 cm
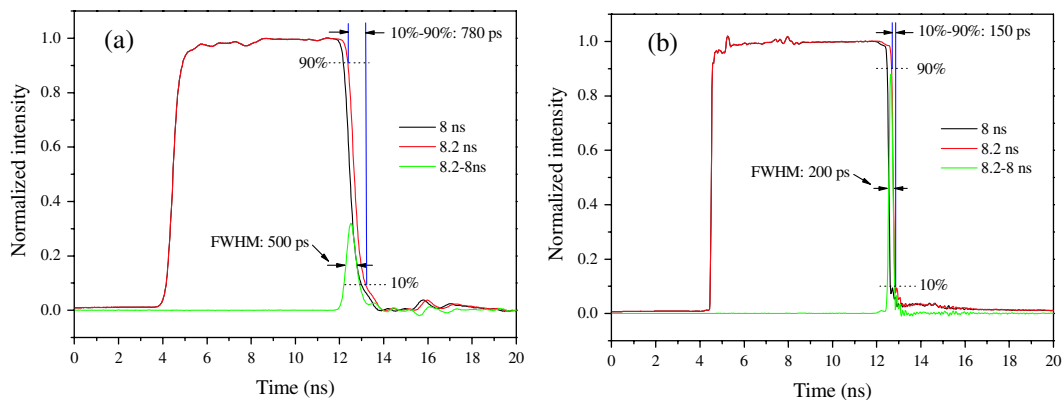

Fig. 4. (Color online) Pulse waveforms of 8 and 8.2 ns pulses generated from (a) pulse generator 1 with a fall-time of 780 ps and (b) pulse generator 2 with a fall-time of 150 ps. The green curves are the differential pulses.
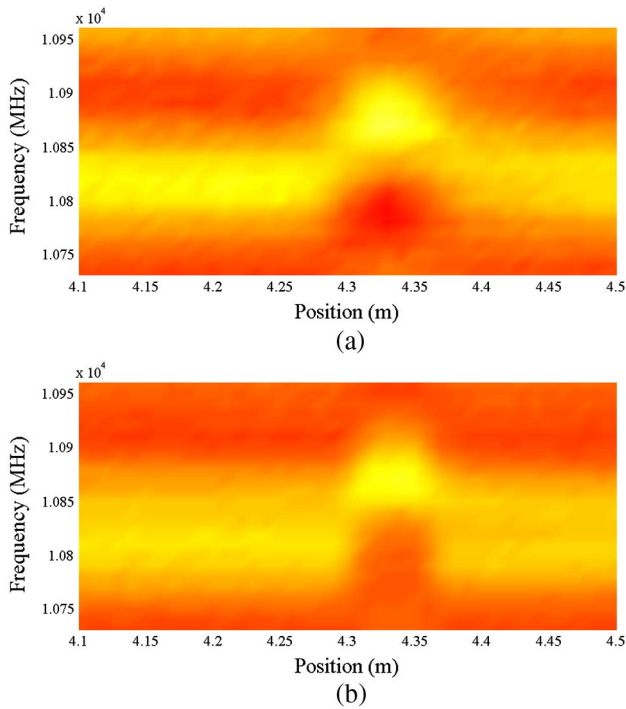
Fig. 5. (Color online) The measured 3-D Brillouin spectra with the 8/8.2 ns pulse pair using (a) pulse generator 1 with a fall-time of 780 ps and (b) pulse generator 2 with a fall-time of 150 ps. A 5 cm segment located at 4.31–4.36 cm was heated to 73 °C.

was heated to 73 °C through the semiconductor Peltier heater. The 3-D Brillouin spectra in the vicinity of the heated segment are shown in Fig. 7(a), where the 2 cm heated segment is clearly shown in the form of the shifted spectra. Figure 7(b) gives the fitted BFS and corresponding temperature, where the measured value of the center point of the heated 2 cm segment matches with the real temperature of 73 °C monitored by a thermocouple, indicating an effective 2 cm spatial resolution.

The measured Brillouin spectra with 8 and 8.2 ns pulses are plotted in Fig. 8(a), in which their differential spectrum is magnified by a factor of 20 for
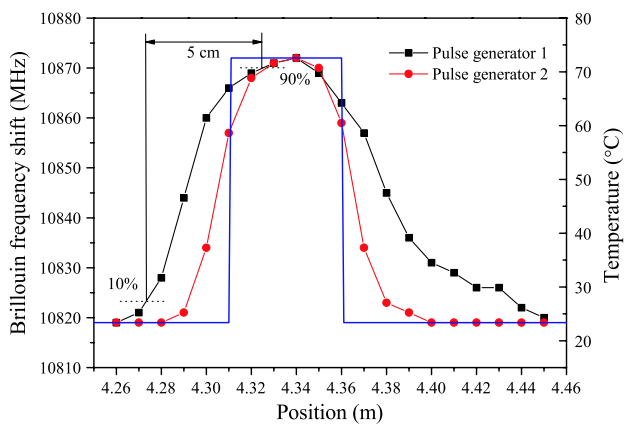

Fig. 6. (Color online) The fitted BFS and corresponding temperature as a function of position for the two cases of Fig. 5. The blue solid line represents the real temperature profile.
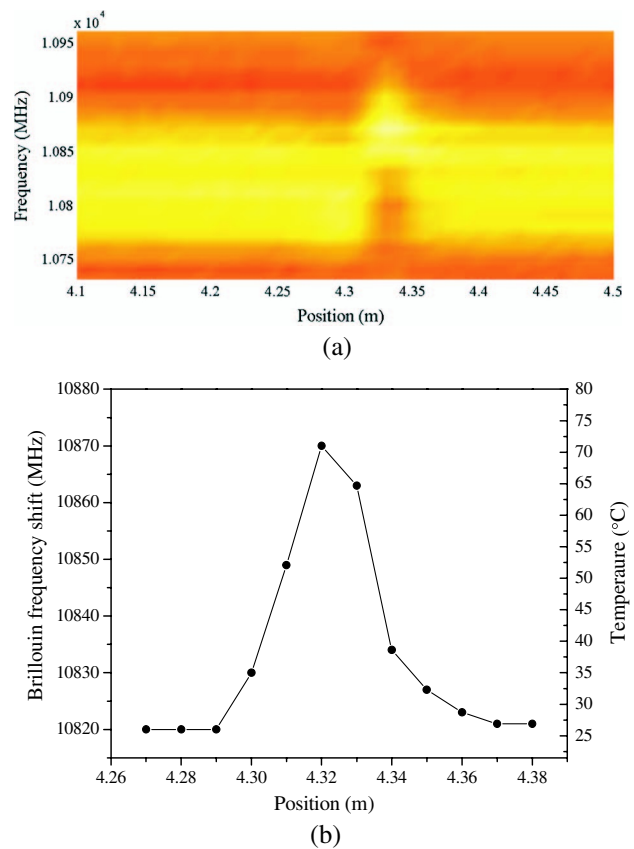

Fig. 7. (Color online) Measured results with the 8/8.2 ns pulse pair using pulse generator 2: (a) the 3-D Brillouin spectra and (b) the fitted BFS and corresponding temperature as a function of position. A 2 cm segment located at 4.33–4.35 cm was heated to 73 °C.

clarity. The experimental results match very well with the simulations as shown in Fig. 8(b). Note that the differential spectrum features two symmetric negative wings and a narrower linewidth. These features are from the pulse spectrum and the differential process. As the measured Brillouin spectrum is the convolution of the natural BGS and the pulse spectrum, it manifests a Lorentz profile when the pulse duration is much larger than the phonon lifetime; when the pulse duration is similar to or smaller than the phonon lifetime, it tends to be dominated by the pulse spectrum. In our case, the 8 and 8.2 ns pulses are around the phonon lifetime in the transient domain; the contribution from the pulses on the Brillouin spectra causes the negative wings after the differential process. The advantage of a narrower spectrum with respect to the original ones is that it can provide higher frequency accuracy.

To verify the capability of long-range sensing, a 2 km single-mode fiber is added in front of the 10 m PM fiber to extend the sensing length. The time traces of the Brillouin signal using a 8/8.2 ns pulse pair over the entire sensing fiber are shown in Fig. 9, where the frequency offset is fixed at the BFS of the single-mode fiber. Note that there are up-thrust and down-thrust signals observed overlapping at the
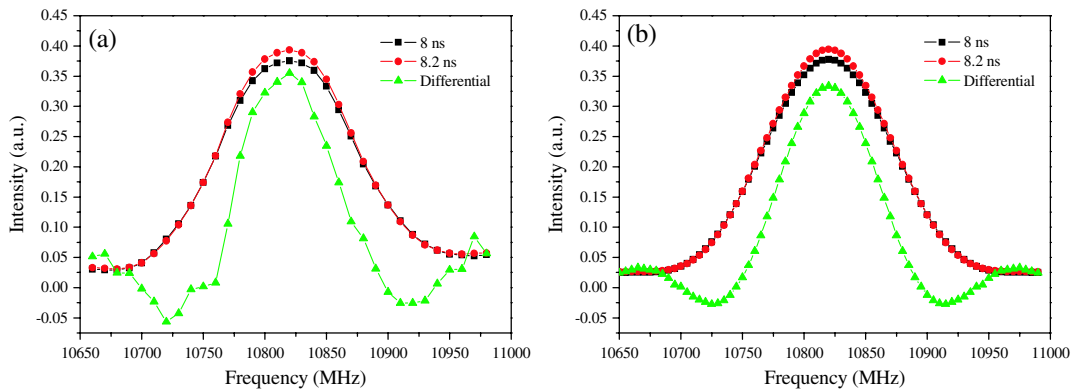
Fig. 8. (Color online) The Brillouin spectra with the 8/8.2 ns pulse pair: (a) experiment and (b) simulation, where the differential signals are magnified by a factor of 20 for both cases.
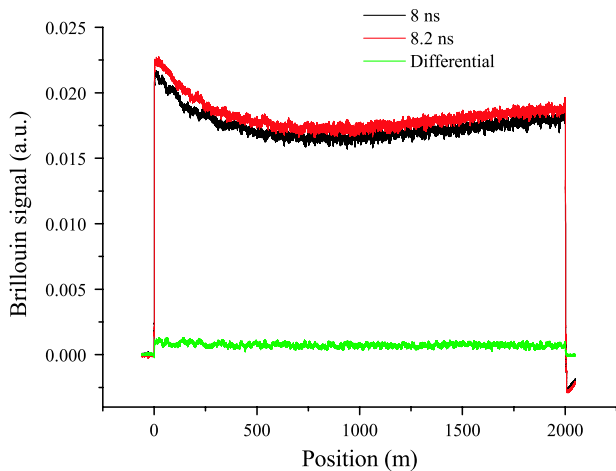

Fig. 9. (Color online) Measured time traces of the Brillouin signal with the 8/8.2 ns pulse pair of a 2 km fiber.
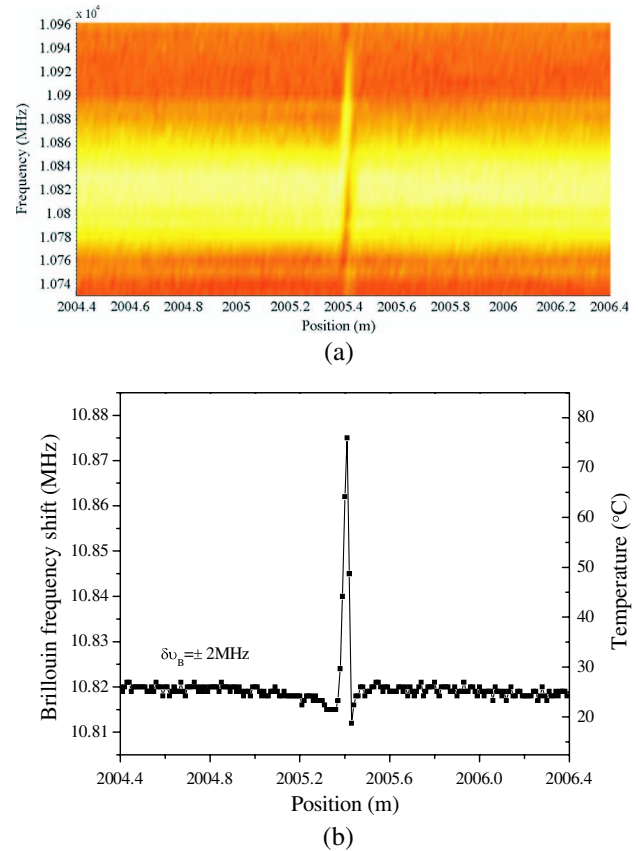

Fig. 10. (Color online) Measured results at the end of the 2 km sensing fiber: (a) the 3-D Brillouin spectra and (b) the fitted BFS and corresponding temperature as a function of position. A 2 cm segment was heated to 76 °C.

front end of and after the Brillouin signal, respectively, which may be caused by the imperfect design of the amplifier circuit of the detector. However, this detrimental signal can be completely removed by the differential process, as shown on the differential signal in Fig. 9.

Near the end of the sensing fiber, a 2 cm fiber segment was heated to 76 °C. The measured 3-D Brillouin spectra in the vicinity of the heated segment are shown in Fig. 10(a), and the fitted BFS and corresponding temperature are plotted in Fig. 10(b), where the measured value of the center point of the heated 2 cm segment matches with the real temperature of 76 °C. The standard deviation of the BFS at the end of the 2 km sensing fiber is calculated to be about 2 MHz, which corresponds to a 2 °C temperature accuracy.

5. Conclusions

First, it is experimentally shown that in DPP-BOTDA the actual spatial resolution is determined by the pulse width of the differential pulse rather than the pulse-width difference of the pulse pair, and it is limited by the fall-time of the original pulses. Second, considering the SNR reduction in a differential signal with respect to the original signals in DPP-

BOTDA, an optimized 8/8.2 ns transient pulse pair with a 150 ps fall-time is used to realize an effective 2 cm spatial resolution; the differential Brillouin spectrum shows a narrower linewidth due to a transient pulse pair and differential process, which can give a better frequency accuracy. In the end, a 2 km sensing length is demonstrated with a 2 cm spatial resolution and a 2° C temperature accuracy.

References

1. K. Shimizu, T. Horiguchi, Y. Koyamada, and T. Kurashima, "Coherent self-heterodyne detection of spontaneously Brillouin-scattered light waves in a single-mode fiber," Opt. Lett. **18**, 185–187 (1993).
2. T. R. Parker, M. Farhadiroushan, V. A. Handerek, and A. J. Rogers, "Temperature and strain dependence of the power level and frequency of spontaneous Brillouin scattering in optical fibers," Opt. Lett. **22**, 787–789 (1997).
3. S. M. Maughan, H. H. Kee, and T. P. Newson, "57 km single-ended spontaneous Brillouin-based distributed fiber temperature sensor using microwave coherent detection," Opt. Lett. **26**, 331–333 (2001).
4. X. Bao, D. J. Webb, and D. A. Jackon, "22 km distributed temperature sensor using Brillouin gain in an optical fiber," Opt. Lett. **18**, 552–554 (1993).
5. M. Nikles, L. Thevenaz, and P. A. Robert, "Simple distributed fiber sensor based on Brillouin gain spectrum analysis," Opt. Lett. **21**, 758–760 (1996).
6. H. Naruse and M. Tateda, "Trade-off between the spatial and the frequency resolutions in measuring the power spectrum of the Brillouin backscattered light in an optical fiber," Appl. Opt. **38**, 6516–6521 (1999).
7. X. Bao, A. W. Brown, M. DeMerchant, and J. Smith, "Characterization of the Brillouin gain/loss linewidth for single mode fibers using very short pulses," Opt. Lett. **24**, 510–512 (1999).
8. A. W. Brown, B. G. Colpitts, and K. Brown, "Dark-pulse Brillouin optical time-domain sensor with 20 mm spatial resolution," J. Lightwave Technol. **25**, 381–386 (2007).
9. T. Sperber, A. Eyal, M. Tur, and L. Thevenaz, "High spatial resolution distributed sensing in optical fibers by Brillouin gain-profile tracing," Opt. Express **18**, 8671–8679 (2010).
10. K. Kishda, C. H. Li, and K. Nishiguchi, "Pulse pre-pump method for cm-order spatial resolution of BOTDA," Proc. SPIE **5855**, 559–562 (2005).
11. F. Wang, X. Bao, L. Chen, Y. Li, J. Snoddy, and X. Zhang, "Using pulse with dark base to achieve high spatial and frequency resolution for the distributed Brillouin sensor," Opt. Lett. **33**, 2707–2709 (2008).
12. Y. Koyamada, Y. Sakairi, N. Takeuchi, and S. Adachi, "Novel technique to improve spatial resolution in Brillouin optical time-domain reflectometry," IEEE Photon. Technol. Lett. **19**, 1910–1912 (2007).
13. L. Thevenaz and S. F. Mafang, "Distributed fiber sensing using Brillouin echoes," Proc. SPIE **7004**, 70043N (2008).
14. W. Li, X. Bao, Y. Li, and L. Chen, "Differential pulse-width pair BOTDA for high spatial resolution sensing," Opt. Express **16**, 21616–21625 (2008).
15. K. Y. Song, S. Chin, N. Primerov, and L. Thevenaz, "Time-domain distributed fiber sensor with 1 cm spatial resolution based on Brillouin dynamic grating," J. Lightwave Technol. **28**, 2062–2067 (2010).
16. K. Y. Song, Z. He, and K. Hotate, "Distributed strain measurement with millimeter-order spatial resolution based on Brillouin optical correlation domain analysis," Opt. Lett. **31**, 2526–2528 (2006).
17. Y. Mizuno, Z. He, and K. Hotate, "One-end-access high-speed distributed strain measurement with 13 mm spatial resolution based on Brillouin optical correlation-domain reflectometry," IEEE Photon. Technol. Lett. **21**, 474–476 (2009).
18. S. M. Foaleng, M. Tur, J.-C. Beugnot, and L. Thevenaz, "High spatial and spectral resolution long-range sensing using Brillouin echoes," J. Lightwave Technol. **28**, 2993–3003 (2010).
19. Y. Dong, L. Chen, and X. Bao, "System optimization of a long-range Brillouin loss-based distributed fiber sensor," Appl. Opt. **49**, 5020–5025 (2010).
20. R. W. Boyd, *Nonlinear Optics*, 4th ed. (Academic, 2008).